Manifestations of Charge Induced Instability in Droplets Effected by Charged Macromolecules

Styliani Consta*
Department of Chemistry, The University of Western Ontario, London, Ontario, Canada N6A 5B7

Anatoly Malevanets
Molecular Structure and Function Program, Hospital for Sick Children, Toronto, Ontario, Canada M5G 1X8

(Received 4 June 2012; published 4 October 2012)

Ion-release processes from droplets that contain excess charge are of central importance in determining the charge-state distributions of macromolecules in electrospray ionization methods. We develop an analytical theory to describe the mechanism of contiguous extrusion of a charged macromolecule from a droplet. We find that the universal parameter determining the system behavior is the ratio of solvation energy per unit length to the square of the ion charge density per unit length. Systems with the same value of the ratio will follow the same path in the course of droplet evaporation. The analytical model is compared with molecular simulations of charged polyethylene glycol macroion in aqueous droplets, and the results are in excellent agreement.

DOI: 10.1103/PhysRevLett.109.148301 PACS numbers: 36.20.Ey, 05.70.Ce, 36.40.Qv, 36.40.Wa

Liquid droplets, that contain excess charge, are ubiquitous in aerosols found in nature and jets produced in electrospray ionization (ESI) methods. ESI has been extensively employed in deposition methods for the coating of surfaces [1–3], in electrospray mass spectrometry for the chemical analysis mainly of biological macromolecules [4–11], and in other spraying technologies such as ink-jet printing and spraying of pesticides. One of the main questions in ESI applications is how the dissolved species emerge from the droplets. When only single ions are present, the instability manifests itself in droplet fissions [12–14]. The droplet fragments when the electrostatic repulsions between ions of the same sign overcome the surface tension that tends to hold the droplet connected. In this situation, the disintegration mechanisms of droplets with excess charge are theoretically described using Rayleigh's model [15] and the ion evaporation model [12,13,16,17]. However, many applications of ESI are concerned with the transfer of charged macromolecules (macroions) from the bulk liquid into the gaseous state via charged droplets. When macroions are present, the charge is covalently or noncovalently bound to the macromolecule. Since the connectivity of the charge prevents droplet fission, the instability has to appear in a different manner from that described by ion evaporation model and Rayleigh mechanisms. Using molecular simulations, we have found that the manifestation of instability in droplet–macroion systems may appear in several ways, therefore, we need more than one theory to describe the various scenarios [18–20]. We have identified three scenarios of charge induced instability in the presence of macroions: contiguous extrusion of the macroion from the droplet [19,20], the pearl model [18], and solvation of the macroion by spiny arrangement of the water solvent around the macroion [18] in order to distribute the charge far from the macroion. To our knowledge, there are no theories that describe the instability of macroion-droplet systems.

In this Letter, we focus on one of the mechanisms of charge instability, the contiguous extrusion of a macromolecule from a droplet. We assume that the charge is localized on the molecule. These conditions are satisfied, for example, in the case of sodiated polyethylene glycol (PEG) molecule in water [19,20]. We develop an analytical theory to study how the parameters of droplet size, length of chain, charge, and solvation energy affect the release mechanisms of a macroions from a droplet. The results of the theory are compared with the molecular simulations of PEG in an aqueous droplet.

In Fig. 1(a) we illustrate the mechanism of extrusion and define the parameters critical to a theoretical examination of the mechanism. The relation of the model to realistic simulations is demonstrated in Fig. 1(b), which shows a typical snapshot of realizations of charged PEG in TIP3P solvent. TIP3P [21] is a standard molecular model for water molecule used broadly in computations. The parameters of the model contributing to the energy are the solvation energy of the linear macromolecule and its charge. In the considered model, we assume that the droplet has spherical shape. The results of the simulations validate this assumption in the case of a charged macromolecule in TIP3P solvent, as shown in Fig. 1(b) and discussed in detail in the next paragraphs. As the droplet shape remains spherical, the surface energy is constant and the surface tension term does not enter Eq. (1). On the basis of the above considerations, we express the total energy of the system as

$$E_{\text{total}} = E_{\text{elec}} + (L - \lambda)\upsilon_0, \tag{1}$$

where L is the length of the macromolecule, λ is the length of the extruded segment of the macromolecule, and υ_0 is the solvation energy per unit length of the macromolecule.

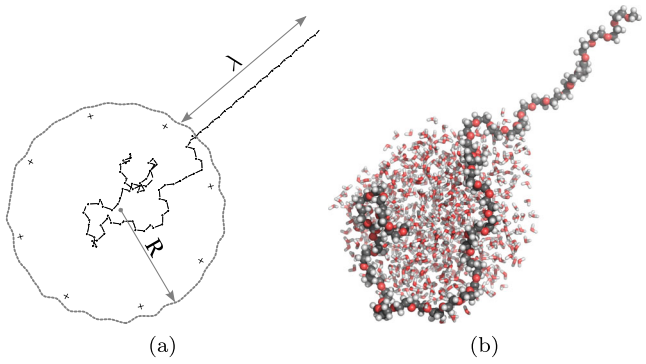

FIG. 1 (color online). Illustration of a system consisting of a partially extruded macromolecule (PEG) in a droplet. (a) Model parameters are defined. The droplet radius is R, and the length of the extruded segment is λ. In a conducting droplet, the electric charges (denoted by "+") are transferred to the isopotential surface of the droplet. (b) Snapshot of a typical conformation of PEG48 chain in a water droplet observed in MD simulations. The droplet consists of 800 water molecules with a coiled segment of PEG molecule. The remainder of the PEG molecule is extended out of the droplet.

Electrostatic energy of the straight rigid segment in vacuum is set to zero, and the corresponding change in the self-interaction energy upon solvation is accounted for by the solvation energy contribution.

We evaluate the electrostatic energy of a conducting sphere and a linear charged macromolecule using macroscopic description of the constituent parts. Using the general formula for the electrostatic energy [[22], see p. 57] electrostatics

$$E_{\text{elec}} = \sum \frac{1}{2} \phi_i' q_i, \tag{2}$$

where q_i are charges and ϕ_i' are electrostatic potentials at the positions of the corresponding charges without that of the charge q_i.

With the use of the technique of electrostatic images, the electrostatic field from charge q at distance x from the conducting droplet is equivalent to a field created by the system of three charges q, $-qR/(R+x)$ at distance $R/(R+x)$ from the center of the sphere and $qR/(R+x)$ at the center of the sphere. Using Eq. (2), we write the contribution to the electrostatic energy from charges in the droplet (which are distributed on the surface) as

$$E_{\text{elec}}(Q_1) = \frac{1}{2} \frac{1}{4\pi\epsilon_0 R} (Q_1 + Q_c) Q_1, \tag{3}$$

where γ is the charge per unit length of the macromolecule, $Q_1 = \gamma(L-\lambda)$ is the charge inside the droplet, and Q_c is the total induced image charge in the center of the droplet given by

$$Q_c = \int_0^\lambda \frac{R\gamma dx}{R+x}. \tag{4}$$

Note, that there is no contribution to the electrostatic energy from the pairs of charges $[q, -qR/(R+x)]$ as they compensate each other exactly on the surface of the sphere.

Contribution to the electrostatic energy from the charges on the extruded part of the macromolecule is

$$E_{\text{elec}}(Q_2) = \frac{1}{2} \frac{1}{4\pi\epsilon_0} \left[(Q_1 + Q_c) \int_0^\lambda \frac{\gamma dx}{R+x} - \int_0^\lambda \int_0^\lambda \frac{\gamma dx}{R + x - \frac{R^2}{R+y}} \frac{R\gamma dy}{R+y} \right]. \tag{5}$$

Adding energies given by Eqs. (3) and (5) and after some algebra, we arrive at

$$E_{\text{elec}} = \frac{1}{2} \frac{1}{4\pi\epsilon_0} \left[\frac{1}{R} (Q_1 + Q_c)^2 - \gamma^2 R \int_0^\lambda \int_0^\lambda \frac{dxdy}{(R+x)(R+y) - R^2} \right]. \tag{6}$$

We analyze the stability of the system given by Eq. (6). The central property is the location of the minima of the energy as a function of macromolecule extrusion λ. The locations of the minima are given by the solutions of the following equations

$$0 = -\frac{\partial E_{\text{total}}}{\partial \lambda} = \upsilon_0 + \frac{1}{4\pi\epsilon_0} \left[\frac{Q_1 + Q_c}{R} \frac{\gamma\lambda}{R+\lambda} + \gamma^2 R \int_0^\lambda \frac{dx}{(R+x)(R+\lambda) - R^2} \right]. \tag{7}$$

Equation (7) can be explicitly evaluated and recast in the following form

$$-\frac{4\pi\epsilon\upsilon_0}{\gamma^2} = \left[\frac{L-\lambda}{R} + \ln\frac{R+\lambda}{R} \right] \frac{\lambda}{R+\lambda} + \frac{R}{R+\lambda} \ln\frac{2R+\lambda}{R}, \tag{8}$$

with dimensionless parameters on both sides of the equation. The universal parameter B_{ex},

$$B_{\text{ex}} = \frac{4\pi\epsilon\upsilon_0}{\gamma^2} = [L\upsilon_0] \left[\frac{Q^2}{4\pi\epsilon L} \right]^{-1}, \tag{9}$$

determines the position of the minima for a specific system. B_{ex} is the ratio of the total solvation energy over a measure of electrostatic energy of the macromolecule and could have been obtained from dimensional analysis as the only combination of two characteristic quantities of the system. The systems with the same ratios of solvation energy to the square of the charge density will follow the same path in the course of droplet evaporation on the $(\lambda/R, L/R)$ diagram.

Following the approach used to describe gas–liquid boundary lines of the van der Waals equation of state, we solved the system of equations $\{\frac{\partial E_{\text{total}}}{\partial \lambda} = 0 \wedge \frac{\partial^2 E_{\text{total}}}{\partial \lambda^2} = 0\}$ and determined that the allowed region of parameters lies on the rhs of the dashed curve shown in Fig. 2 and is given by

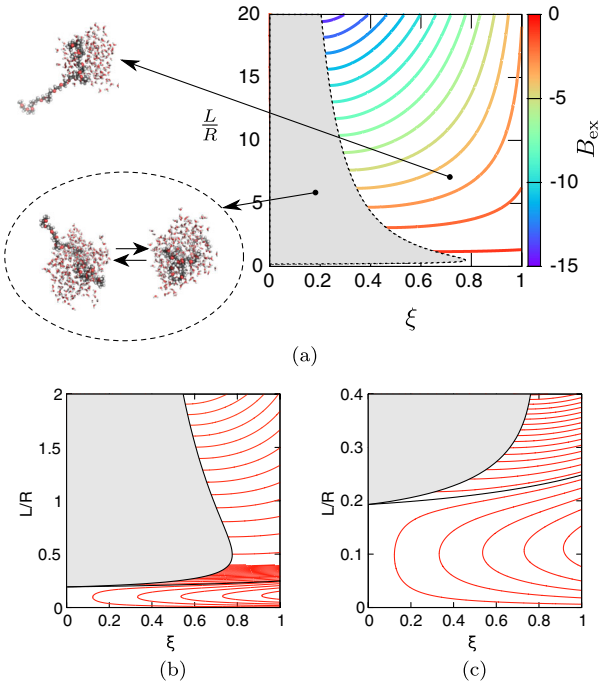

FIG. 2 (color online). Regions of the phase diagram in the system of $\xi = \lambda/L$ and L/R coordinates. Contiguous lines correspond to constant values of the interaction parameter B_{ex}. The gray region in all subplots indicates location of the restricted domain (see details in the text). Subplot (a) shows an overall view of the minima of the droplet energy. Representative snapshots of simulations of charged PEG in water droplets that correspond to the various regions of the phase diagram are also shown. Subplots (b) and (c) show details of specific domains on the diagram. Region 1 corresponds to the area above the thick black line (excluding the shaded area) shown in subplots (b) and (c), and region 2 corresponds to the area below.

$$\frac{L}{R} = \frac{\lambda}{R} + \frac{\lambda^2}{R^2} - \ln\frac{R+\lambda}{2R+\lambda} - \frac{R+\lambda}{2R+\lambda}. \qquad (10)$$

Equations (7) and (10) are conveniently presented in the $(\xi = \lambda/L,\ L/R)$ system of coordinates. The system of equations was solved numerically, and the results of calculations are presented in Fig. 2. On the phase diagram (Fig. 2), the dashed line delineates the region of $(\xi,\ L/R)$ values with the solutions corresponding to the maxima of the total energy (Eq. (1)). In this region the fully solvated chain (corresponding to $\xi = 0$) and an extruded state lying on the boundary of the allowed region are in dynamic equilibrium, as illustrated in the Fig. 2(a) lower inset. On the phase diagram, we identified two distinct regions that correspond to different extrusion mechanisms.

Region 1.—Solving Eq. (10) for $\lambda = 0$, we arrived at the critical value $L/R(\text{critical}) = \ln(2) - 1/2 \approx 0.193$ and the corresponding value of $B_{ex} = -0.69315$. Figure 2(a) shows the isolines for systems with $B_{ex} \leq -0.69315$.

When λ (and ξ) is zero, the macromolecule is in a fully solvated state and is contained inside the droplet. Accordingly, value $\xi = 1$ indicates position of the macromolecule on the surface. Escape of a chain segment from a droplet starting at $\xi = 0$ and progressing to $\xi = 1$, above the critical value, involves an initial transition step, which is an activated process. The subsequent evolution of the system proceeds contiguously along the isolines plotted in Fig. 2. The two states in the activated process correspond to a fully solvated chain in the droplet and a conformation with partially exposed chain lying on the dashed line given by Eq. (10). Typical snapshots of the transition are shown in Fig. 2(a) (snapshots surrounded by the oval region) from simulations of charged PEG in water. The system undergoes critical transformation at the position on the phase diagram determined by intersection of constant B_{ex} and corresponding L/R lines. Manifestations of the transition between the two states were observed in MD simulations and are presented in detail in Fig. 3.

Region 2.—Region 2 is shown by the isolines in Figs. 2(b) and 2(c). The feature of these isolines that distinguishes them from the isolines in region 1 is the looping that they exhibit. If we follow the path with $R \gg L$ $(R/L \to 0)$, the isolines correspond to values of ξ close to one; therefore, the entire macroion lies on the surface of the droplet. As evaporation proceeds and the droplet shrinks below a critical radius, the molecule can be partially solvated (looping of the isolines). The solvation energy will determine the portion of the macroion that will be solvated. Once the lower critical radius point is crossed, the macroion is again pushed out of the droplet. The interesting finding here is that the solvation of this surfactant molecule is possible only in the intermediate regime of finite-size droplets when the electrostatic interactions of a charge with the droplet compensate the negative energy of solvation. This mechanism can be plausibly realized in experiments by chemical modification of the macromolecule, which will lead to an increase of the charge per unit length of the macroion in the course of droplet evaporation. The sodiation of PEG molecule and protonation of peptide side chains are examples of such chemical reactions that will subsequently lead to the macromolecule expulsion. The chain of events is as follows: droplet evaporation, increase of ionic strength, chemical transformation of the macromolecule, and expulsion of the modified molecule from the droplet.

The theoretical model derived above has been validated in numerical experiments of droplets containing charged PEG in water (Fig. 3). Simulations were carried out using the CHARMM molecular modeling package [23]. Water clusters were simulated using TIP3P model [21]. Cutoff free electrostatic interactions were used to model long-range interactions.

Initial conformations were created by equilibrating a PEG macromolecule for 2 ns in a nanodroplet environment. The nanodroplets of water contained a number of solvent molecules above the Rayleigh limit. Initial nanodroplets

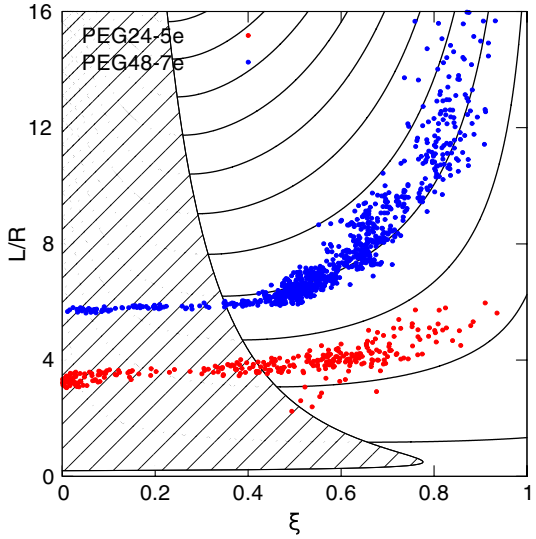

FIG. 3 (color online). Ratio of the chain length to droplet radius versus ξ observed in the computational experiments with simulated evaporation events. In the figure, the experimental values for ejection of PEG48 with charge $+7e$ (upper set of dots) and PEG24 with charge $+5e$ (lower set of dots) from a TIP3P water droplet were superimposed on the theoretical curves (solid lines).

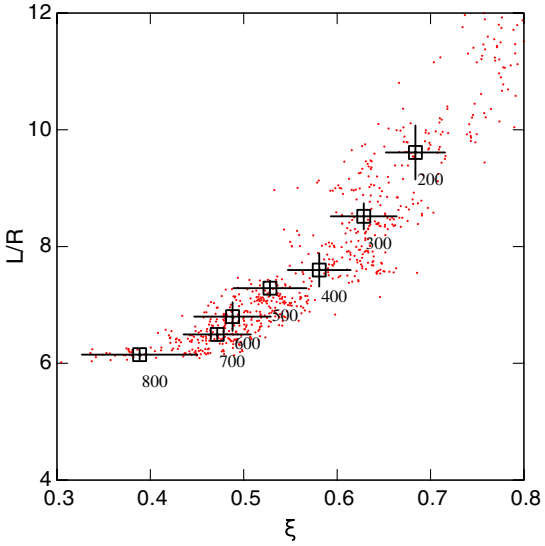

FIG. 4 (color online). Ratio of the chain length to droplet radius (L/R) versus ξ in MD simulations with constant number of solvent molecules (black squares with error bars) and evaporation calculations (red dots). In the plot, red dots correspond to instantaneous values of (L/R, ξ) taken every 5 ps during the run with simulated evaporation events. The square points with x and y error bars show average positions and the error of the plot variables in the course of MD run with a fixed number of solvent molecules.

containing PEG24, PEG36, and PEG48 in 800 TIP3P water molecules were produced.

Charges on the macromolecule were modeled by *smearing* the charge uniformly over the main chain atoms of the macromolecule. We investigated systems with total charge $Q = 7e$ and $Q = 5e$. Constant temperature MD runs were carried out by coupling the models to the Berendsen thermostat. Conformations of the macromolecule were subsequently sampled from evaporation simulations wherein the solvent molecules were randomly removed from the cluster and the system was allowed to relax to a new steady state. The total length of simulations was 4.0 ns for TIP3P. We verified that the cluster conformations in the evaporation run were sampled from the equilibrium ensemble by carrying out simulations with fixed number of solvent molecules at several reference points. The results of 1 ns simulations for 100, 200, 300, 400, 500, 600, 700, and 800 solvent molecules demonstrated agreement between equilibrium and quasi-static "evaporation" simulations.

In the simulations, we defined a droplet as a connected cluster of solvent molecules. In the droplet we also included the atoms of the chain that lie within 4.8 Å radius of the solvent molecules comprising the cluster. The radius of the droplet was computed from the radius of gyration of the selected atoms and by using the relation between the radius R_{gyr} of a solid sphere and its radius R

$$R_{\mathrm{gyr}} = \sqrt{\frac{3}{5}}R. \tag{11}$$

The length of the extended segment was calculated by finding the maximum distance of the atoms of the chain from the center of mass of the droplet, defined above, less the radius of the droplet.

In Fig. 4, values of (ξ, L/R) obtained in equilibrium MD simulations with fixed number of TIP3P molecules are superimposed on those calculated in evaporation experiments. The results are in complete agreement, confirming the validity of the results obtained in quasistatic evaporation experiments. We would like to draw attention to the calculated values of the parameters with 800 TIP3P molecules. The fraction of the extruded chain shows the largest magnitude of fluctuations. We attribute enhancement of fluctuations at this point to a bimodal free-energy profile. The corresponding two states are the fully solvated and partially extruded conformations. The extent of the extrusion is calculated from the intersection of parameter L/R for solvated chain and the boundary of the restricted region plotted in Fig. 2.

In the course of solvent removal, the chain extrusion steadily increases. We superimposed calculated values of degree of extrusion and ratio L/R on the phase diagram of Fig. 2. The results are shown in Fig. 3. The evaporation curve follows positions of the minima of the free energy given in Eq. (10). The curve demonstrates remarkable agreement with theoretical calculations. As the size of droplet decreases, the fluctuations become more pronounced, as expected due to finite size effects. As the size of the droplet

falls below tens of molecules, the cluster definition breaks down. The connected solvent cluster becomes strongly aspherical and disconnected. This behavior is captured in enhanced fluctuations of the monitored parameters at values of ξ exceeding 0.8.

In conclusion, we developed a theoretical model for contiguous extrusion of a charge macromolecule from a droplet. The key finding of the theory is that the universal parameter determining the system behavior is the ratio of solvation energy to the square of the ion charge density of the macromolecule. Under certain conditions, the expulsion of the macroion was found to be an activated process. The simulations revealed a new mechanism of ion evaporation that differs from conventional charge residue [4] and ion-evaporation mechanisms. It may explain the charged states of noncompact macromolecules observed in electrospray mass spectrometry experiments that yield charges above that given by the Rayleigh model [24–29].

S. C. acknowledges a Discovery Grant from the Natural Sciences and Engineering Research Council of Canada (NSERC) for funding and SHARC-Net for computing facilities.

*styliani.constas@gmail.com

[1] V. N. Morozov and T. Y. Morozova, Anal. Chem. **71**, 3110 (1999).
[2] V. Bergeron, D. Bonn, J. Y. Martin, and L. Vovelle, Nature (London) **405**, 772 (2000).
[3] O. Wilhelm, L. Madler, and S. E. Pratsinis, J. Aerosol Sci. **34**, 815 (2003).
[4] M. Dole, L. Mack, R. Hines, R. Mobley, L. Ferguson, and M. Alice, J. Chem. Phys. **49**, 2240 (1968).
[5] P. Kebarle and U. H. Vererk, Mass Spectrom. Rev. **28**, 898 (2009).
[6] E. Segev, T. Wyttenbach, M. T. Bowers, and R. B. Gerber, Phys. Chem. Chem. Phys. **10**, 3077 (2008).
[7] T. Wyttenbach and M. T. Bowers, Annu. Rev. Phys. Chem. **58**, 511 (2007).
[8] J. F. de la Mora, B. A. Thomson, and M. Gamero-Castano, J. Am. Soc. Mass Spectrom. **16**, 717 (2005).
[9] E. Williams, J. Mass Spectrom. **31**, 831 (1996).
[10] P. Schnier, D. Gross, and E. Williams, J. Am. Soc. Mass Spectrom. **6**, 1086 (1995).
[11] S. Nguyen and J. B. Fenn, Proc. Natl. Acad. Sci. U.S.A. **104**, 1111 (2007).
[12] S. Consta, J. Mol. Struct. **591**, 131 (2002).
[13] S. Consta, K. Mainer, and W. Novak, J. Chem. Phys. **119**, 10125 (2003).
[14] K. Ichiki and S. Consta, J. Phys. Chem. B **110**, 19168 (2006).
[15] L. Rayleigh, Philos. Mag. **14**, 184 (1882).
[16] J. Iribarne and B. Thomson, J. Chem. Phys. **64**, 2287 (1976).
[17] B. Thomson and J. Iribarne, J. Chem. Phys. **71**, 4451 (1979).
[18] S. Consta, J. Phys. Chem. B **114**, 5263 (2010).
[19] S. Consta and J. K. Chung, J. Phys. Chem. B **115**, 10447 (2011).
[20] J. K. Chung and S. Consta, J. Phys. Chem. B **116**, 5777 (2012).
[21] W. Jorgensen, J. Chandrasekhar, J. Madura, R. Impey, and M. Klein, J. Chem. Phys. **79**, 926 (1983).
[22] E. Guggenheim, Proc. R. Soc. A **155**, 49 (1936).
[23] B. Brooks, R. Bruccoleri, B. Olafson, D. States, S. Swaminathan, and M. Karplus, J. Comput. Chem. **4**, 187 (1983).
[24] T. Nohmi and J. Fenn, J. Am. Chem. Soc. **114**, 3241 (1992).
[25] J. Fenn, J. Rosell, T. Nohmi, S. Shen, and F. Banks, in *Biochemical and Biotechnological Applications of Electrospray Ionization Mass Spectrometry*, edited by A. Snyder, ACS Symposium Series (American Chemical Society, Washington, DC, 1996), Vol. 619, pp. 60–80.
[26] J. F. de la Mora, Anal. Chim. Acta **406**, 93 (2000).
[27] M. Samalikova and R. Grandori, J. Mass Spectrom. **40**, 503 (2005).
[28] S. H. Lomeli, S. Yin, R. R. O. Loo, and J. A. Loo, J. Am. Soc. Mass Spectrom. **20**, 593 (2009).
[29] H. J. Sterling and E. R. Williams, J. Am. Soc. Mass Spectrom. **20**, 1933 (2009).